Conformal Antennas on Liquid Crystalline Polymer Based Rigid-Flex Substrates Integrated With the Front-End Module

Nevin Altunyurt, *Student Member, IEEE*, Ralf Rieske, Madhavan Swaminathan, *Fellow, IEEE*, and Venkatesh Sundaram

***Abstract*—Recent developments in liquid crystalline polymer (LCP)-based processing technology have shown that highly-integrated, fully-packaged radio-frequency (RF) front-end modules with high-performance can be designed by using the system-on-package (SOP) approach. However, the direct integration of a large antenna element to a small module package still remains an issue. This paper presents a novel conformal antenna structure, which results in a compact integration of the antenna and the module package for 5 GHz WLAN/WiMAX applications. The extension of 5 GHz single-band operation to 2.4/5 GHz dual-band operation is also discussed in this paper. The antenna is an inverse L-shaped monopole printed on a 25-μm-thick flexible LCP layer, which protrudes from a rigid multilayer organic substrate. The shielding effects of a grounded metal case, which can house the associated module circuitry, are also considered during the design process. The metal case serves as a vertical ground plane for the antenna in addition to protecting the module circuitry from the near-fields of the antenna. The flexible LCP substrate can be bent and folded over the module case, resulting in a compact design and the tight integration of the antenna with the front-end module. The details of the design and the fabrication of the proposed structure as well as the simulation and the measurement data are presented in this paper.**

***Index Terms*—Antennas, conformal antennas, flexible antennas, integrated mobile antennas, liquid crystalline polymer (LCP), WiMAX antennas, WLAN antennas.**

I. Introduction

FUTURE wireless communication systems require increased functionality in smaller and more reliable modules while providing improved performance without increasing the manufacturing costs. As an alternative to the system-on-chip (SOC) approach, the system-on-package (SOP) approach has shown potential to provide a reliable packaging solution for future radio-frequency (RF) modules. SOP addresses possible integration problems, such as substrate isolation and substrate loss, by using low-loss organic dielectrics suitable for RF applications.

Recent advances in the liquid crystalline polymer (LCP)-based multilayer organic processing technology have made LCP a promising candidate for RF SOP applications. In addition to being a low-cost dielectric for a large panel area fabrication process, LCP has a combination of good electrical and mechanical properties. LCP has a low dielectric constant of $\varepsilon_{\mathrm{r}} = 2.95$ and a low loss-tangent of 0.002 up to millimeter wave frequencies. LCP also has favorable mechanical properties such as mechanical flexibility, a low coefficient of thermal expansion, and low moisture absorption [1], [2]. Furthermore, LCP has the mechanical strength to be the final printed wiring board (PWB), making it an excellent packaging substrate for SOP applications.

Previous work on RF SOP has shown that high-performance front-end modules with significant size reduction can be designed by 3-D integration of RF front-end functional blocks into LCP-based multilayer organic substrates. Examples of a filter, low noise amplifier (LNA), voltage controlled oscillator (VCO), and mixer designs using embedded passives in multilayer substrates can be found in the literature [2]–[8]. However, the SOP-integration of antennas with the front-end module with high-efficiency and low-cost is still a significant problem. In this paper, a novel configuration to enable high-level integration of a conformal monopole antenna to the front-end module for WLAN/WiMAX operation is proposed. The proposed configuration is explained for the single-band and the dual-band antenna operation by using an inverse L-shaped monopole antenna. The co-design of the antenna with the module package is also studied in this paper by considering the effects of the on-package shielding metal case.

This paper is organized as follows. In Section II, the antenna integration problem is studied by considering the prior work in this area. In Section III, the proposed conformal antenna concept on rigid-flex substrate is explained for the single-band operation with the details of the fabrication of the prototype. Measurement and simulation results for the single-band antenna are also presented in Section III. The extension of the single-band operation to the dual-band operation is discussed in Section IV. Simulation and measurement results for the dual-band operation are also included in Section IV, followed by the conclusion in Section V.

Manuscript received May 26, 2008; revised December 16, 2008. This work was recommended for publication by Associate Editor L.-T. Hwang upon evaluation of the reviewers comments.

N. Altunyurt, M. Swaminathan, and V. Sundaram are with the School of Electrical and Computer Engineering, Georgia Institute of Technology, Atlanta, Georgia 30332 USA.

R. Rieske is with the Technische Universitaet Dresden, D-01062 Dresden, Germany (e-mail: nevin@ece.gatech.edu).

Color versions of one or more of the figures in this paper are available online at http://ieeexplore.ieee.org.

Digital Object Identifier 10.1109/TADVP.2009.2020517

II. Antenna Integration

Compact and efficient integration of the antenna to the front-end module is still a major problem although the miniaturization of the module alone has been achieved by using multilayer topologies with novel interconnection technologies. One reason for this problem is the large size of the antenna due to its necessary electrical length. The size of the antenna is particularly an issue for the microwave frequency range used by the most of the wireless mobile applications (1–6 GHz). Another difficulty arises because of the undesired coupling between the antenna and the module circuitry as the distance between the two is reduced. This results in a need for the co-design of the antenna with the module circuitry or the package to prevent possible detuning of the antenna or the RF circuits after integration [9].

Despite the difficulties mentioned above, the integration of the antenna directly on the module package has the advantages of reduced loss and size. Integrating the antenna on the module package can also eliminate the mismatch introduced by the coaxial cable connections along with the associated loss and the cost of the cable. Moreover, the overall performance of the system can be improved since the stringent design rules, such as 50 Ω input/output matching, can be relaxed with the integration. Thus, there is a need for a novel technology to miniaturize the front-end module with the antenna integrated directly on the module package.

The most straightforward method for integrating the antenna to the module is to place the antenna at a distant location away from the circuits and to create the connection with a coaxial cable. This method is widely utilized in the state-of-the-art mobile devices, where the antenna or multiple antennas are placed along the edges of the case of the mobile device, and the RF signals are carried through a long, lossy coaxial cable. Although this method is straightforward, the cable introduces mismatch and conductor losses into the system. In an application of this method to printed antennas, the antenna is printed on the package leaving a separation with the rest of the circuitry to avoid undesired coupling at the expense of leaving unused package space, which conflicts with the miniaturization objective behind the integration.

A more compact method for the integration is to use the 3-D stacking approach of the low-temperature co-fired ceramic (LTCC) technology, where a patch antenna is printed on top of the module circuitry [9]–[11]. A metal plane or a cavity between the antenna and the circuit components can be used as the shielding mechanism in this configuration. Since vertical real estate is used in this approach, this configuration usually results in an increase in the overall height of the package. Thin substrates or substrates with high dielectric constants can be used to decrease the thickness of the package. However, achieving wide-band and high-efficiency operation becomes harder for these cases.

The advantage of the LTCC integration method stems from the fact that it is a multilayer technology. Therefore, both the module circuitry and the antenna can be integrated into the package. However, LTCC is a more expensive solution for RF SOP applications compared to the multilayer organic-based technology having the same integration capability. Additionally, the mismatch of the coefficient of thermal expansion of LTCC with that of the PWB can lead to reliability issues in highly-integrated front-end packages. Moreover, the ceramic-based LTCC package is not strong enough to be used as the final PWB. As an alternative to LTCC, LCP-based multilayer organic technology offers a low-cost, low-profile, high-performance RF SOP solution with FR-4 compatible processes.

The advantages of multilayer substrates in miniaturizing the front-end module size by using embedded passives can be combined with the flexibility of the LCP to find a solution for the antenna integration problem. Conformal antennas fabricated on LCP-based rigid-flex substrates can provide a promising solution to the antenna integration problem in SOP applications [12], [13]. As shown in Fig. 1, previous work on LCP-based substrates is extended in this paper to include the on-package integration of the antenna. Emergent technologies such as wearable electronics or nanotechnology-based foldable electronics can also benefit from the low-cost flexible antenna configuration explained in this paper. This rigid-flex configuration, explained for the LCP in this paper, can also be applied to other flexible organic materials capable of being used in multilayer substrates.

The idea of using conformal antennas on flexible substrates for consumer applications has been studied previously, examples of which can be found in [14]–[16]. In these papers, single and dual-band antennas on several flexible substrates are proposed. Nevertheless, unlike the low-cost 3-D multilayer technology proposed in this paper, none of the previous work on flexible antennas has provided a complete solution, where the integration of the module circuitry can also be handled successfully. Moreover, the fabrication of the flexible antennas proposed so far mostly includes costly high-temperature procedures; e.g., the dual-band antenna on silicon suspended parylene membrane uses a MEMS-based fabrication procedure including high-temperature processes [14].

The proposed multilayer module concept, including the antenna integrated on the module package, is shown in Fig. 2. As seen in Fig. 2, the antenna is printed on a thin flexible LCP layer, which protrudes from a rigid multilayer stack-up. The rigid part of the substrate includes module components such as filters, mixers, VCOs, baluns, LNA and the matching circuitries realized by using embedded passives printed on different layers of the substrate. The power amplifier (PA) and the transceiver chip are placed on the top layer of the rigid substrate and enclosed by an on-package shielding metal case, which serves as a part of the front-end module package. The antenna is printed on the flexible part of the substrate and folded over the metal case to result in a compact integration. The antennas explained in this paper are optimized to be used in the folded antenna position; however, the flexible LCP layer can also be used in other configurations illustrated with the dashed lines in Fig. 2.

As mention earlier, a mechanism is required to protect RF circuits from the radiated fields of the antenna when the antenna is integrated in close proximity to the module. In this proposed configuration, the conventional on-board shielding metal case is replaced with an on-package shielding metal case to eliminate

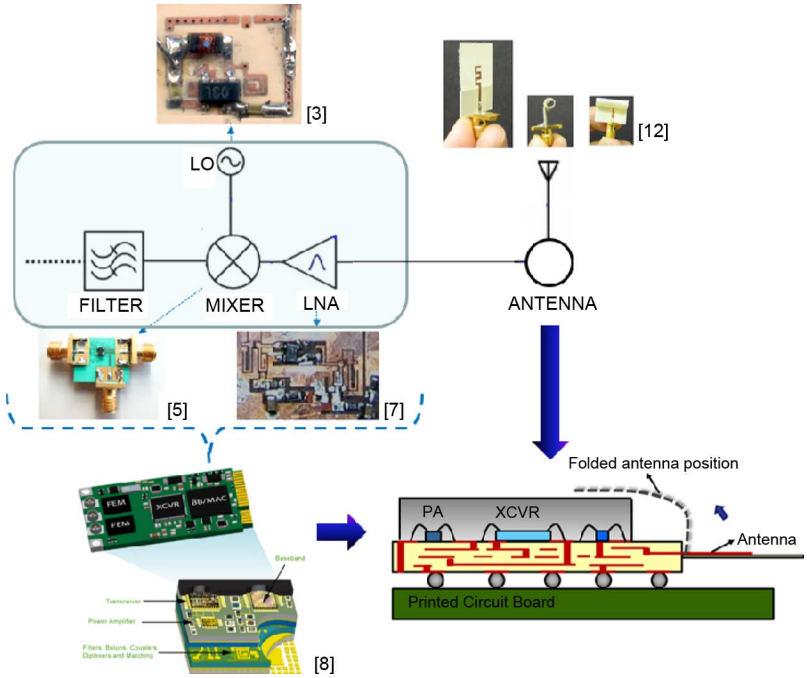

Fig. 1. Extension of the RF receiver front-end on a multilayer organic-based package to include on-package antenna integration.

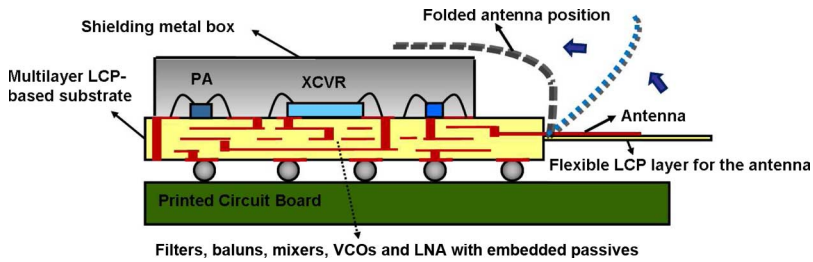

Fig. 2. Proposed multilayer module concept using the conformal antenna on a flexible layer of LCP. The abbreviations used in the figure stand for power amplifier (PA) and transceiver (XCVR).

the need for a separation between the module circuitry and the antenna. The on-package shielding metal case is also employed in [17], where a bent-monopole antenna is placed on the side of the shielding metal box. The antenna used in [17] is a separate metal piece soldered to a feeding line on the package. This connection method introduces mismatch into the system while adding a connection step into the integration. Moreover, the integration of the antenna with the rest of the front-end circuitry still remains an issue since, contrary to the conformal antenna proposed in this paper; the antenna analyzed in [17] is not printed on the same substrate with the module circuitry.

III. Conformal Antennas on Rigid-Flex Substrates

A. Structure Description

In this section, a single-band WLAN/WiMAX antenna for 5 GHz operation is introduced. The antenna substrate is a multilayer, balanced, rigid-flex substrate composed of three layers of low-loss dielectrics, as shown in Fig. 3. In this stack-up a 25-μm -thick LCP layer is supported by 508-μm-thick top and bottom glass-reinforced organic dielectric layers (prepreg layers). The LCP layer has a dielectric constant of 2.95 and a loss-tangent of 0.002. The prepreg layers have a loss-tangent of 0.0037 and a dielectric constant of 3.48.

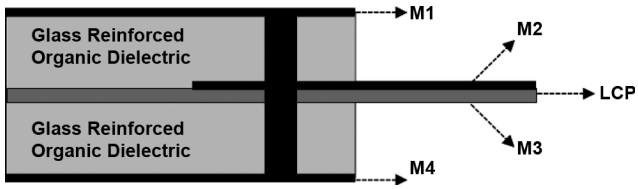

Fig. 3. Cross section of the balanced stack-up used for the proposed structure.

The substrate consists of a flexible part for the antenna, and a rigid part for the signal lines and the module circuitry as shown in Fig. 2. The 30 mm$\times$45 mm LCP layer is between the 30 mm$\times$ 33 mm rigid prepreg layers. This middle LCP layer protrudes from one edge of the substrate; thus, providing a 12-mm-long flexible substrate for the antenna due to the mechanical flexibility of the LCP.

As seen from the cross section of the substrate shown in Fig. 3, there are four metal layers in this stack-up (M1–M4). The antenna is fabricated on the protruded portion of M2, so that it can be bent, folded, or even rolled resulting in a compact

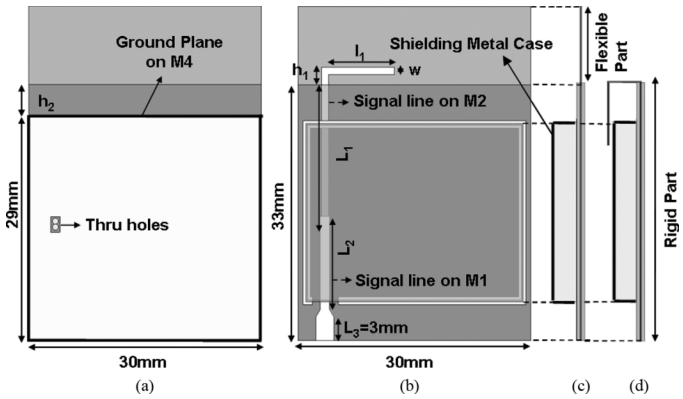

Fig. 4. Details of the proposed single-band antenna structure integrated with the module case. (a) Bottom view, (b) Top view, (c) Side view, (d) Folded side view.

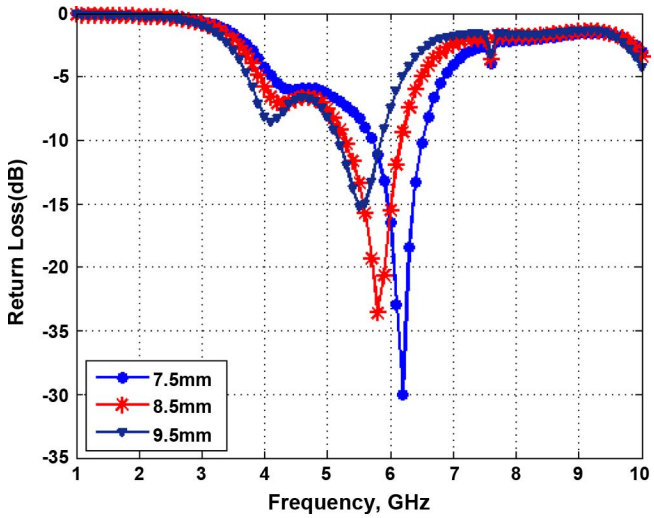

Fig. 5. Simulated return loss for different values of l_1 ($h_1 = 2.3$ mm and $h_2 = 4$ mm).

design. The microstrip signal lines feeding the antenna are on M1 and M2. Metal layer M4 serves as the ground reference for the signal lines and the antenna. M3 is left unused in this design.

The antenna structure used in this design is an inverted L-shaped monopole since it can provide wide operation bandwidth with a relatively small size. The details of the proposed antenna structure, integrated with the shielding metal case serving as the module package, are presented in Fig. 4. As shown in Fig. 4(b), the antenna consists of an L-shaped structure with width, $w = 1$ mm; length, $l_1 = 8.5$ mm; height, $h_1 = 2.3$ mm; and an embedded part, $h_2 = 4$ mm. This embedded part is the portion of the signal line on metal layer M2 that is not covered by the bottom ground plane. The antenna is excited through a 50-Ω microstrip line printed along the rigid part of M2 with length $L_1 = 19$ mm. The signal line on M2 is connected to another 50-Ω signal line on M1, with $L_2 = 12$ mm, by two through holes to enable the use of an edge-mount SMA connector for the measurements. The through holes are isolated from the ground plane by a rectangular clearance area as shown in Fig. 4(a). The widths of the 50-Ω signal lines on M1 and M2 are 1.2 mm and 0.9 mm, respectively. These values were found by considering the traces to be in a stripline configuration due to the presence of the grounded metal box. Similarly, a tapered transition is used at the edge of the substrate to account for the changes in the impedance in the absence of the metal box.

The shielding metal case is a hollow metal box with a size of 28 mm $\times$ 23 mm $\times$ 3 mm, constructed by bending an 80 μm thick copper sheet. The metal box is electrically connected to a rectangular metal trace printed on metal layer M1, which is shorted to ground by a series of through holes. The metal box not only protects the module circuitry from the undesired coupling to the nearby conducting elements and radiated fields of the antenna, but it also serves as a ground reference for the antenna.

B. Design Based on Simulation

A commercial 3-D FEM-based electromagnetic simulator, the high frequency structure simulator (HFSS) [18] was used to optimize the proposed structure. The antenna was designed to be used in the folded configuration, in which the protruding flexible LCP portion is folded over the shielding metal case, as shown in Fig. 2 and Fig. 4(d).

It was found during the design process that the primary parameters affecting the matching and the resonant frequency of the antenna are the length of the antenna, l_1, the height of the antenna, h_1, and the distance of the bottom ground plane to the antenna, h_2, as shown in Fig. 4. A series of parametric sweep simulations were performed to study the effects of these parameters on the matching of the antenna.

The simulated return loss data obtained for three different values of antenna length, $l_1 = 7.5$ mm, 8.5 mm, and 9.5 mm with $h_1 = 2.3$ mm and $h_2 = 4$ mm, is shown in Fig. 5. The resonance frequency of the antenna decreases as the length of the L-shaped radiating structure, l_1, is increased. This is expected due to the increase in the electrical length of the antenna, as l_1 is increased. Furthermore, it can be observed that the bandwidth and the matching level of the antenna are also affected as the length l_1 is changed. This may be because of the change in the capacitive coupling between the antenna and the vertical ground provided by the metal box.

For the fixed value of $l_1 = 8.5$ mm, the effect of the antenna height, h_1, was studied by simulating the structure for $h_1 = 2.3$ mm, 4 mm, and 5 mm. The distance from the ground, h_2, was kept as 2.5 mm in these simulations. As seen from Fig. 6, the resonance frequency of the antenna is shifted to higher frequencies as the height h_1 is decreased while the bandwidth remains approximately unchanged for these three cases.

Finally, the effects of the distance from the ground, h_2, is studied by simulating the structure for $h_2 = 2.5$ mm, 3 mm, and 4 mm with $l_1 = 8.5$ mm and $h_1 = 2.3$ mm. As shown in Fig. 7, the distance h_2 affects both the bandwidth and the resonance frequency of the antenna. As a result of these simulations, the final values for the fabricated structure were chosen as $l_1 = 8.5$ mm, $h_1 = 2.3$ mm, and $h_2 = 4$ mm to cover the 5 GHz WLAN and WiMAX bands. It was found from the parametric sweeps for h_1 and h_2 that both h_1 and h_2 change the resonance frequency of the antenna. This means that both h_1 and h_2 contribute to the resonant electrical length of the antenna. The total

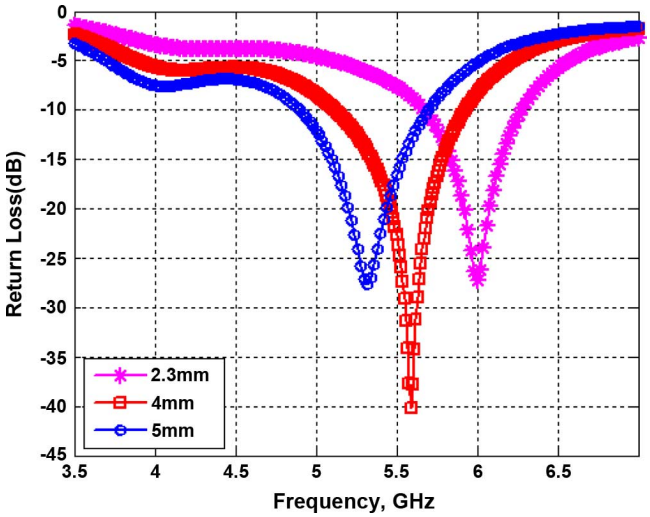

Fig. 6. Simulated return loss for different values of h_1 ($h_2 = 2.5$ mm and $l_1 = 8.5$ mm).

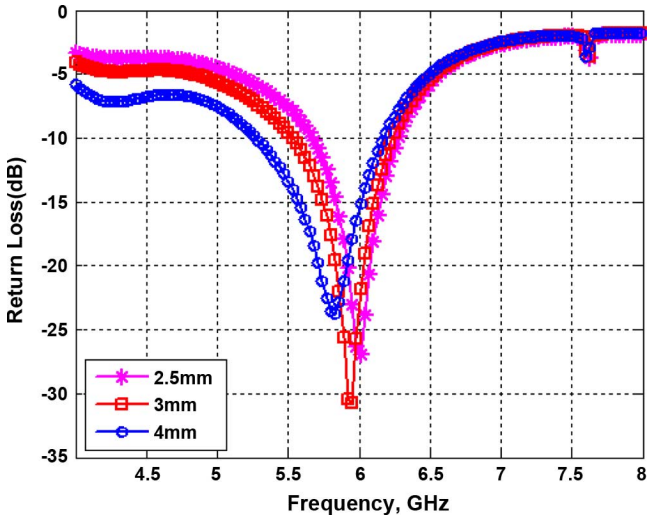

Fig. 7. Simulated return loss for different values of h_2 ($h_1 = 2.3$ mm and $l_1 = 8.5$ mm).

length, $L = l_1 + h_1 + h_2$, of the optimized design is found to be approximately $0.28\lambda_o$ at a resonant frequency of 5.8 GHz.

C. Fabrication

The antennas presented in this paper were fabricated using a novel low-cost multilayer rigid-flex LCP process [19]. This proprietary process technology employs solely low-temperature FR-4 compatible processes (all $< 200\,^{\circ}\mathrm{C}$). It allows for ceramic-like near-hermetic packaging with enhanced reliability by utilizing organic dielectrics with extremely low moisture uptake.

As mentioned earlier, a 25-μm-thick LCP layer was used for the antenna signal traces and the resonating structures. Multiple layers of a low-loss glass-reinforced adhesive dielectric were bonded with the LCP to form the rigid part of the substrate. The antennas presented in this paper were fabricated on a stack-up with only three layers of dielectrics as a proof-of-concept. The

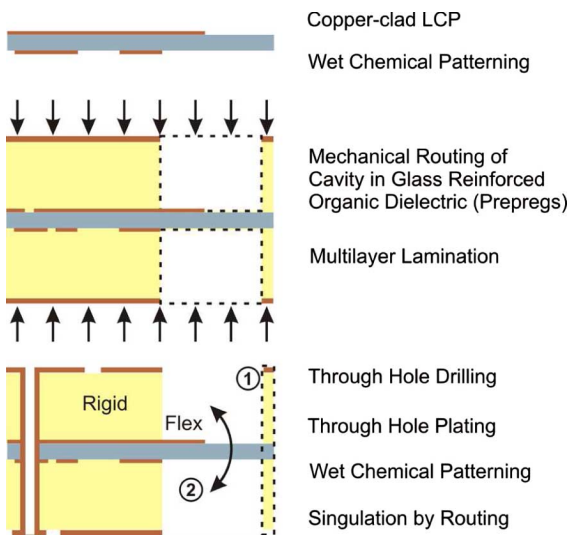

Fig. 8. Process flow diagram for the rigid-flex antenna substrate.

number of substrate layers can be increased, as in [2] and [3], to create more real estate for the embedded passives realizing the module circuitry. The thickness of the substrate and the position of the ground shielding can also be adjusted based on the thickness and the number of the prepreg and the LCP layers. If necessary by the application, even the rigid part of the substrate can be made more flexible by changing the number and the thickness of the laminate layers.

The fabrication of the rigid-flex antenna substrate follows the process flow chart shown in Fig. 8. The first step of the process is patterning the metal layer M2 and M3 on the LCP core layer. Next, the cavities above and below the antenna structures were formed by precision mechanical routing of the prepreg layers. The prepreg layers were placed on a board with alignment pins, as shown in Fig. 9, to prevent misplacement problems. Five layers of 101.6-μm-thick prepreg layers were used on each side of the LCP layer to realize the 508 μm thickness on each side. The LCP layer was placed between the prepreg layers as shown in Fig. 9(b) and (c). Two copper layers were also placed on the top and the bottom of the stack-up, as shown in Fig. 9(c), to realize the metal layers M1 and M4 in Fig. 3. Similar to the prepreg layers, cavities were drilled on these copper layers. The alignment step was followed by the multilayer lamination ($< 200\,^{\circ}\mathrm{C}$) to bond the LCP with the adhesive prepreg layers.

After the multilayer lamination step, through holes were mechanically drilled and plated by using both electroless and electrolytic copper plating to form vertical interconnections. Patterning of the metal layers M1 and M4 was done by wet chemical processing. Finally, the antenna elements were singulated by precision mechanical routing. The panels were fabricated on $9\mathrm{in} \times 12\mathrm{in}$ format using large-area PWB tooling, resulting in a low-cost implementation that can be easily scaled to larger panel sizes for further cost reduction.

The photos of the fabricated prototype are presented in Fig. 10. The metal box and the SMA connector were mounted on the substrate as shown in Fig. 10(b). Then, the flexible substrate of the antenna was folded over the metal case as seen

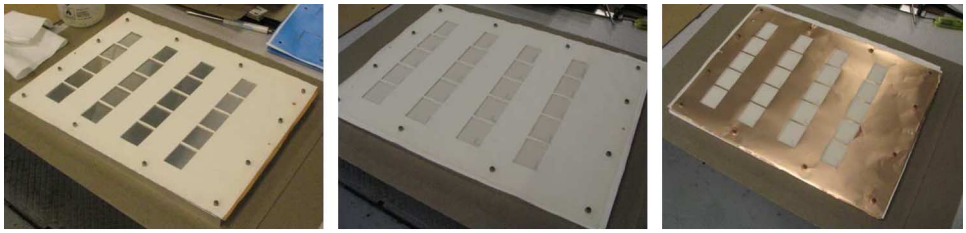

(a) (b) (c)

Fig. 9. Photographs of the alignment step during fabrication. (a) Bottom prepreg layers placed on the alignment board after forming the cavities. (b) Total stack-up including the middle LCP layer and the top prepreg layers. (c) The metal copper layer placed to form metal layer M4.

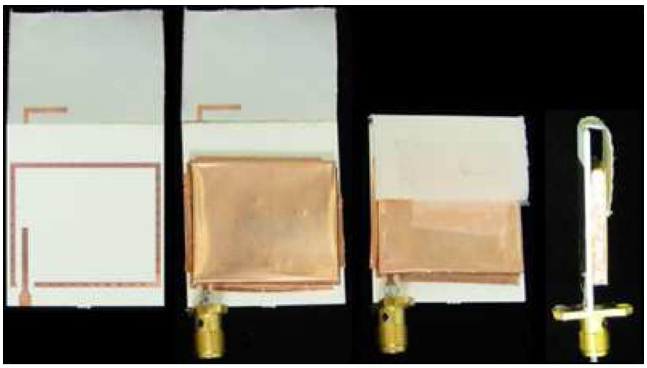

(a) (b) (c) (d)

Fig. 10. Photographs of the fabricated prototype. (a) Antenna. (b) Antenna with the metal case. (c) Folded configuration. (d) Side view of the folded antenna.

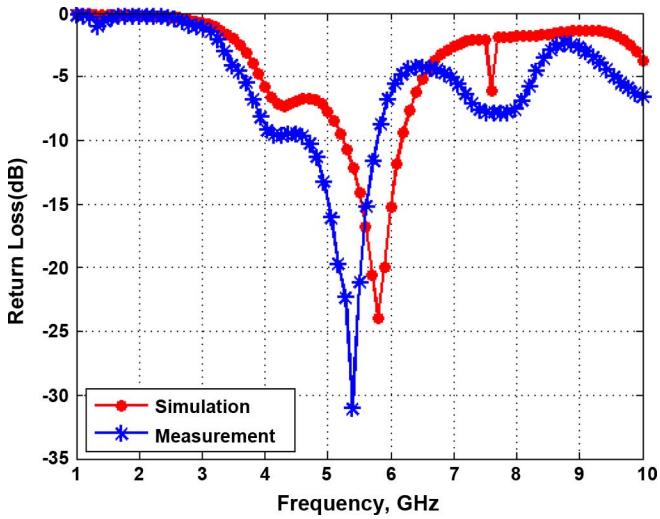

Fig. 11. Simulated and measured return loss of the single-band antenna.

in Fig. 10(c). The side view of the folded configuration is also shown in Fig. 10(d).

D. Design Verification by S-Parameter and Far-Field Measurements

To verify the performance of the proposed flexible antenna configuration, a prototype was fabricated and measured. Fig. 11 shows the simulated and measured results for the return loss of the fabricated antenna. As seen in Fig. 11, good agreement is observed between the measured and the simulated results. The measured 10 dB bandwidth of the antenna is 1070 MHz (4710 MHz–5780 MHz) covering most of the 5 GHz WLAN (5150 MHz–5825 MHz) and WiMAX bands (5250 MHz–5850 MHz). The return loss value at the upper band of the WiMAX band is measured to be $-8.5\,\mathrm{dB}$, which is an accepted value for wireless applications.

The reason behind the small shift in the measured resonance frequency of the antenna was investigated using a series of simulations, where the fabrication tolerances for the via misplacement and the signal misalignment were modeled. It was found from these simulations that the return loss of the antenna is not affected considerably from the misalignment of the signal lines on metal layers M1 and M2 or the misplacement of the critical via connections between these signal lines. Another possibility considered as the reason of the shift in the measured resonance frequency of the antenna was the difference between the folding of the flexible substrate in the fabricated prototype and in the HFSS model.

The difference in the folding can be explained as a result of the enlargement of the prepreg layers toward the cavities, as shown in Fig. 12, because of the pressure and the heat applied during the multilayer lamination step of the fabrication. The enlargement of the prepreg layers increases the separation between the antenna and the ground plane, labeled as h_2 in Fig. 4(a), and decreases the height of the L-shaped resonator, labeled as h_1 in Fig. 4(b), from the values of the optimized design. This, in turn, changes the capacitive coupling of the antenna to the ground plane and the shielding metal box, whose effect is observed as a shift in the resonance frequency of the antenna. The change in the resonance frequency can be avoided by compensating for the enlargement of the prepreg layers when mechanically routing the cavities before lamination.

The effect of the enlargement of the prepreg layers was captured with an HFSS simulation, where the width of the rigid part of the substrate was increased by 0.5 mm to model the enlargement of the prepreg layers. In this simulation, the $h_1 + h_2$ summation was kept the same with the value in the optimized design. The comparison of the return loss is shown in Fig. 13. As seen in the figure, when the folding is further away by 0.5 mm, the resonance frequency of the antenna decreases similar to the measured return loss. This result supports the idea that the shift in the measured resonance frequency of the antenna is due to the enlargement of the prepreg layers during the multilayer lamination step.

The resonance observed around 7.6 GHz in both the simulation and the measurement data in Fig. 11 is the box resonance corresponding to the dominant TM mode of a partially loaded

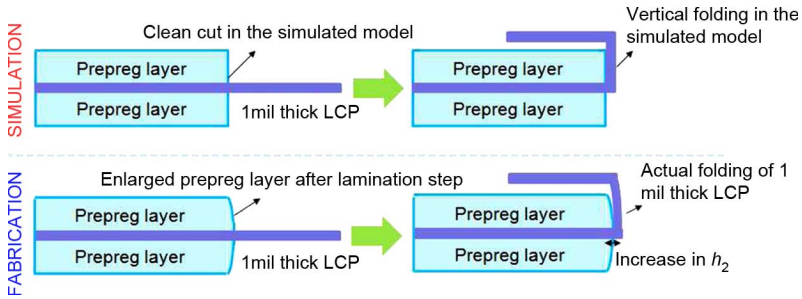

Fig. 12. Comparison of the cross-sections of the stack-up in the simulation model and the fabricated prototype. The pressure and the heat applied in the lamination step result in the enlargement of the prepreg layers toward the cavities. This enlargement affects the folding of the flexible substrate.

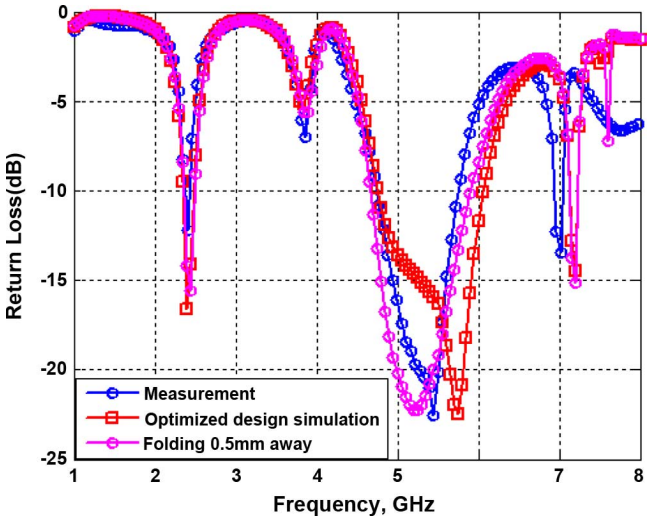

Fig. 13. Return loss comparison of the antenna to observe the effect of the enlargement of the prepreg layer.

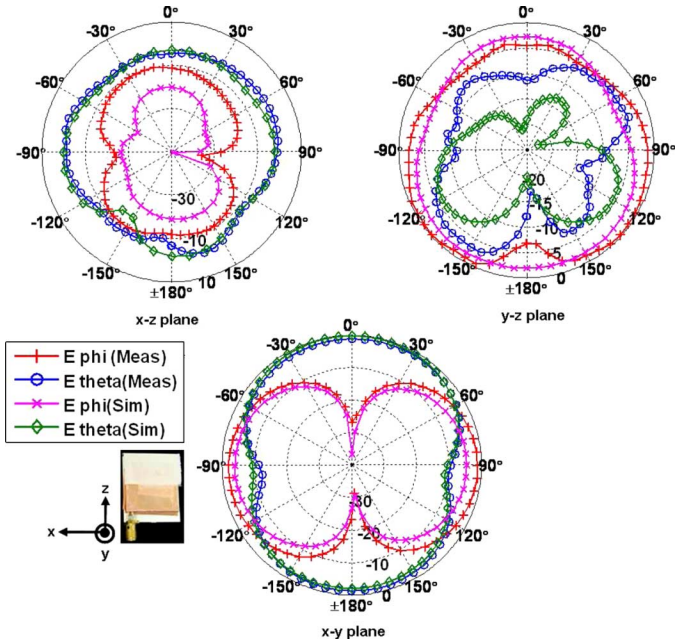

Fig. 14. Simulated and measured radiation pattern of the single-band antenna at 5.2 GHz.

rectangular cavity resonator with a size of 23 mm × 28 mm × 4 mm [20], [21]. Since the shielding metal box is shorted to ground with a series of vias, the box acts like a closed rectangular cavity partially filled with the rigid substrate of the proposed structure. It should be noted that the box resonance frequency falls out of the band of interest as desired.

The far-field of the fabricated antenna was also measured at 5.2 GHz. The simulated and measured radiation patterns of the antenna in the *x*–*y*, *y*–*z*, and *x*–*z* plane are shown in Fig. 14. As seen in Fig. 14, the measured patterns agree well with the simulation results. The correlation between the measured and the simulated results is particularly good for the *x*–*y* plane since the effects of the SMA connector are eliminated in the *x*–*y* plane. It should also be noted that, the overall radiation pattern of the antenna has a nearly omni-directional pattern, which is desirable for mobile applications. The radiation pattern has two slight nulls along approximately $\varphi = 45°$ and $\varphi = 135°$ owing to the fact that the radiating structure is composed of three orthogonal resonators, labeled as l_1, h_1, and h_2 in Fig. 4. The measured and simulated peak gains of the antenna at 5.2 GHz are 1.74 dBi and 2.75 dBi, respectively. The slight difference may be attributed to the SMA connection and the cable errors introduced in the measurement.

E. Comparison With the Rigid Substrate

The single-band L-shaped antenna was redesigned on a totally rigid substrate to observe the advantages of the conformal configuration explained in this section. The stack-up in Fig. 3 was used as the rigid substrate without the protruding part. Fig. 15 shows the details of the both antenna designs on rigid-flex and totally rigid substrates side-by-side. The antenna is on metal layer M2 in both designs. However, the antenna is embedded in the substrate for the rigid substrate case; whereas, it is positioned on the flexible portion for the rigid-flex substrate. The dimensions of the signal lines and the metal box are the same with the values provided for the rigid-flex antenna explained previously.

The final dimensions of the antenna on the rigid substrate was found as $l_1 = 5$ mm, $L_1 = 22.5$ mm, and $h_2 = 6.5$ mm with a substrate area of 30 mm × 39 mm. Since the conformal antenna on the rigid-flex substrate is designed to be used in the folded configuration, as shown in Fig. 15(e), the final size of the rigid-flex structure is determined only with the size of the rigid part of the substrate, which is 33 mm × 30 mm. These values

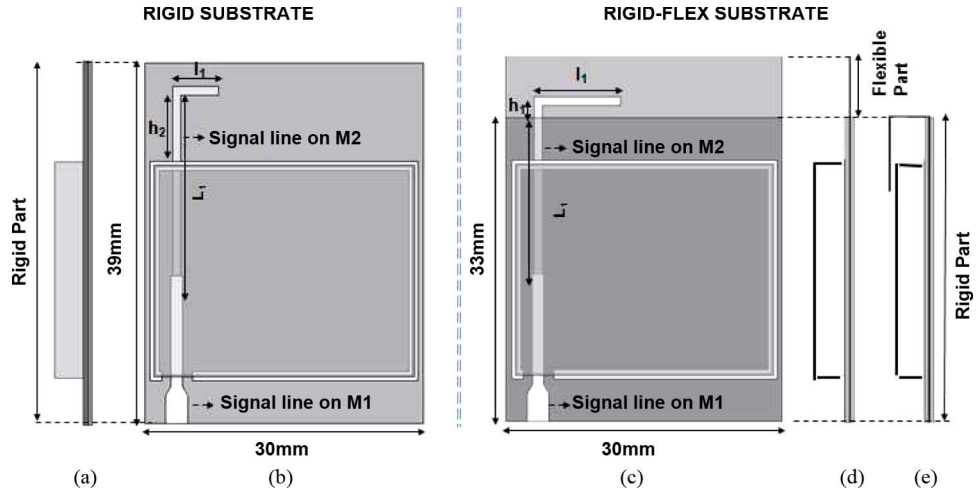

Fig. 15. Comparison of the single-band L-shaped antenna designs on rigid and rigid-flex substrates. (a) Side view (rigid). (b) Top view (rigid). (c) Top view, straight (rigid-flex). (d) Side view, straight (rigid-flex). (e) Side view, folded (rigid-flex).

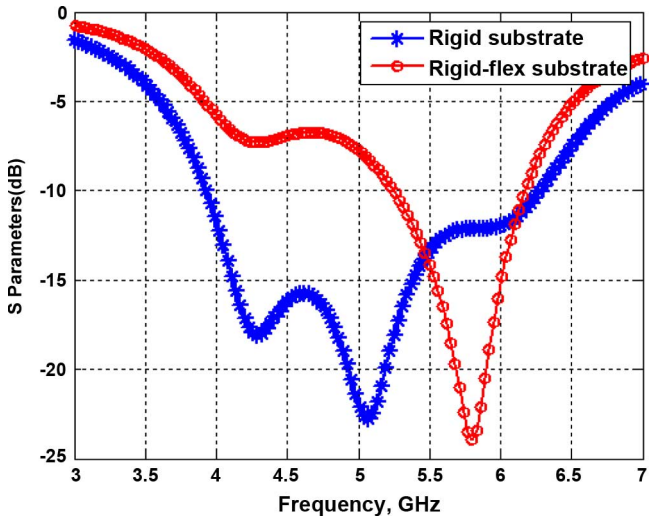

Fig. 16. Return loss comparison of the single-band L-shaped antenna designs on rigid and rigid-flex substrates.

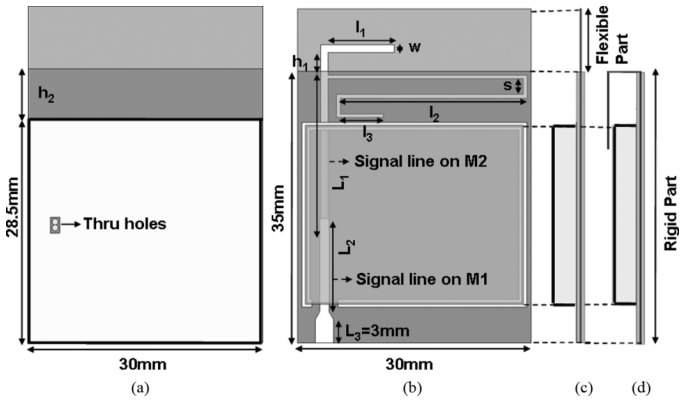

Fig. 17. Details of the proposed dual-band antenna structure integrated with the module case. (a) Bottom view. (b) Top view. (c) Side view. (d) Folded side view.

show that a 6 mm decrease in the width of the substrate can be achieved by making use of the flexibility of the LCP substrate.

The comparison of the simulated return loss values of both antennas are presented in Fig. 16. As seen in the figure, the antenna on the totally rigid substrate has a wider bandwidth than that of the conformal antenna on the rigid-flex substrate. The wider bandwidth is a result of two merging resonances created by the parts of the antenna labeled as l_1 and h_2 in Fig. 15(b). The part labeled as h_2 in Fig. 15(b) represents the part that is not covered with the ground plane. Therefore, this part also acts like a monopole antenna and creates a resonance close to that of the part labeled as l_1.

The far-field of the antenna on the rigid substrate was also simulated. It was found that both designs have similar far-field patterns. The simulated peak gain of the antenna on the rigid substrate at 5.5 GHz was found as 3.2 dBi compared to 2.9 dBi of the conformal antenna.

IV. Dual-Band Antenna for 2.4/5 GHz WLAN Band

A. Structure Description

The single-band antenna discussed in Section III was transformed to a dual-band antenna such that the operation frequency covers both the 2.4 GHz and 5 GHz WLAN bands. This was achieved by including an additional radiating structure resonating at 2.4 GHz. The compactness of the design was preserved by choosing the second radiator as a meandered structure. The unoccupied separation area between the antenna and the ground plane, labeled as h_2 in Fig. 4, was used by embedding the second radiator in the rigid part of the substrate. This way, a dual-band antenna was designed with only a 2 mm size increase in one of the linear dimensions between the single-band and the dual-band structure.

The details of the final dual-band antenna are shown in Fig. 17. The dual-band antenna was printed using the same stack-up with the single-band antenna as shown in Fig. 3. The meandered structure was embedded in the rigid part of the same metal layer, M2, with the inverse L-shaped monopole as shown in Fig. 17.

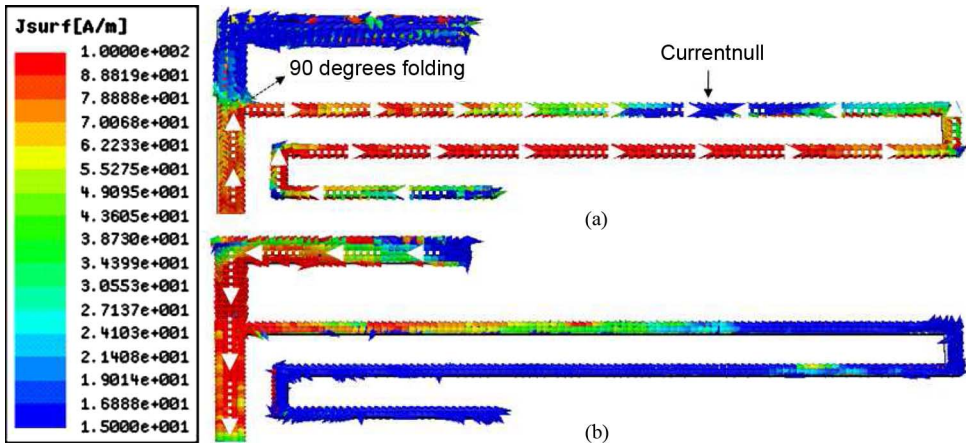

Fig. 18. Surface current distribution of the proposed dual-band antenna in folded configuration at (a) 2.4 GHz and (b) 5.2 GHz.

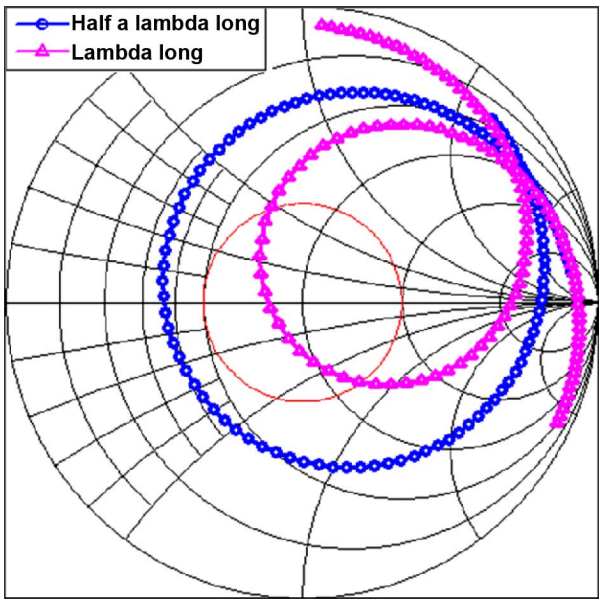

Fig. 19. Return loss comparison of a λg long and a $\lambda g/2$ long structures on Smith chart.

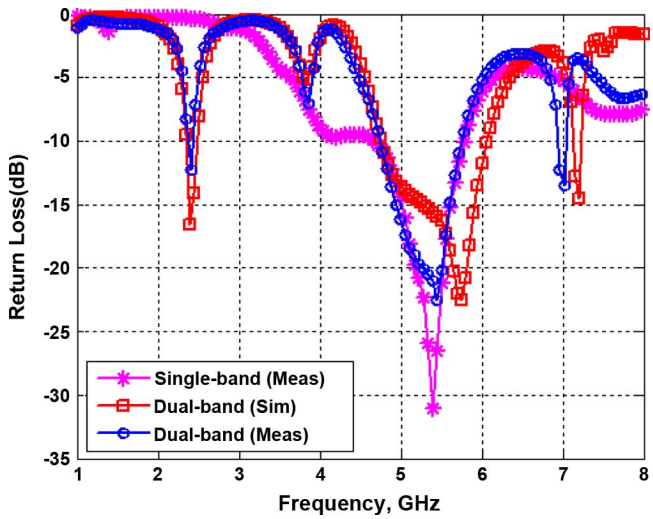

Fig. 20. Simulated and measured return loss of the 2.4/5 GHz dual-band antenna.

B. Design Based on Simulation

Similar to the single-band antenna explained in Section III, the optimization of the dual-band antenna performance for the folded configuration was done using HFSS. Fig. 18 shows the surface current distribution of the antenna in the folded configuration at 2.4 and 5.2 GHz. The substrate layers are made invisible in the figure to show the current distribution on the embedded meander resonator. As seen in Fig. 18, the currents on the L-shaped resonator are stronger at 5.2 GHz; whereas, the meander resonator has stronger currents at 2.4 GHz. The current distribution in Fig. 18(b) implies that the meander is a one-guided-wavelength-long (λ_g) resonator at 2.4 GHz with a current null separating two $\lambda_g/2$ long sections.

Although a half-a-wavelength-long structure can also provide the desired resonance, a full-wavelength-long resonator was preferred to achieve the necessary 10 dB bandwidth in the 2.4 GHz band. As seen from the Smith chart shown in Fig. 19, the real part of the input impedance of the half-a-wavelength-long resonator antenna is lower than the full-wavelength-long structure, resulting in poor matching. The matching of the half-a-wavelength-long structure can be improved by increasing the separation from the ground plane, labeled as h_2 in Fig. 17. However, this conflicts with the aim of the miniaturization. A more valid solution for a fully integrated system, such as one shown in Fig. 2, is replacing the conventional $50\,\Omega$ matching impedance with another impedance value such that both the antenna and the duplexer are optimized simultaneously. The antenna size can be further decreased with this approach while improving the performance.

A 50-Ω matching was followed in the design of the antenna prototype since a 50-Ω edge-mount SMA connector was used during measurements. As seen in Fig. 19, the full-wavelength resonator can be well-matched to 50-Ω in the VSWR $= 2$ circle. The optimization of the antenna for the 2.4 GHz operation frequency was done by tuning the separation between the arms of the meander and the total length of the meandered structure while the design rules obtained in Section III was applied to optimize the antenna operation in the 5 GHz band. The final

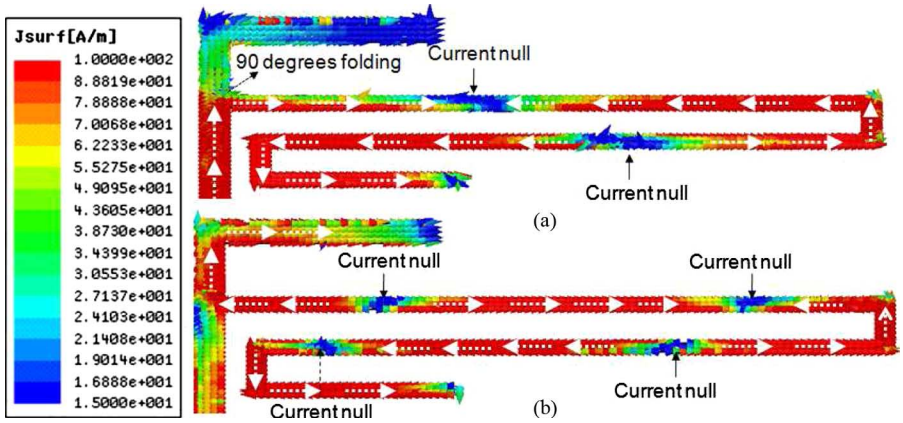

Fig. 21. Surface current distribution of the proposed dual-band antenna at (a) 3.7 GHz and (b) 7 GHz.

values of the parameters shown in Fig. 17 can be listed as follows: $l_1 = 8.5$ mm, $h_1 = 2.5$ mm, $h_2 = 6.5$ mm, $w = 1$ mm, $s = 2$ mm, $l_2 = 24$ mm, $l_3 = 5.5$ mm, $L_1 = 21$ mm, $L_2 = 12$ mm, and the width of the meandered line is 0.5 mm. The lambda long length of the antenna can be verified by calculating the length of the current-path as $L = h_2 + l_2 + 2s + l_3 = 64$ mm, which is equal to $0.98\lambda_g$ at 2.45 GHz.

C. Design Verification by S Parameter and Far-Field Measurements

The simulated and measured return loss results of the conformal dual-band antenna are shown in Fig. 20. The measured return loss of the single-band antenna is also included in Fig. 20 for comparison. The 2.4 GHz band created by the meandered resonator is clearly seen in the figure. The measured 10 dB bandwidths of the dual-band antenna are 90 MHz (2435–2445 MHz) for the 2.4 GHz band and 1000 MHz (4750–5750 MHz) for the 5 GHz WLAN band. The bandwidth of the antenna in the 2.4 GHz band can be improved by slightly decreasing the end length, l_3, or increasing the separation between the arms of the meander, s. As in the case of single-band antenna, a slight shift in the resonance frequency is observed in the 5 GHz band due to the enlargement of the prepreg layers affecting the folding of the antenna.

The additional resonances seen in Fig. 20 at 3.7 and 7 GHz correspond to the resonances of the meander structure when it is $1.5\lambda_g$ and $2.5\lambda_g$ long. This can be seen from the surface current distributions of the meander structure at 3.7 and 7 GHz as shown in Fig. 21. As seen in Fig. 21(a), there are two current nulls separating $\lambda_g/2$ long sections at 3.7 GHz. The resonance at 7 GHz is supported with the currents on both the L-shaped resonator and the meander, and there are four current nulls on the meander structure. The resonance at 3.7 GHz can be avoided by replacing the full-wavelength-long meander resonator with a half-a-wavelength-long resonator; however, this was not possible due to the limitations in the matching of the antenna as mentioned earlier. A resonance around 7 GHz is observed even when a half-a-wavelength-long resonator is used.

The radiation patterns of the dual-band antenna were also measured at 2.4 GHz and 5.2 GHz. The results are presented in Fig. 22. Similar to the single-band antenna, good correlation

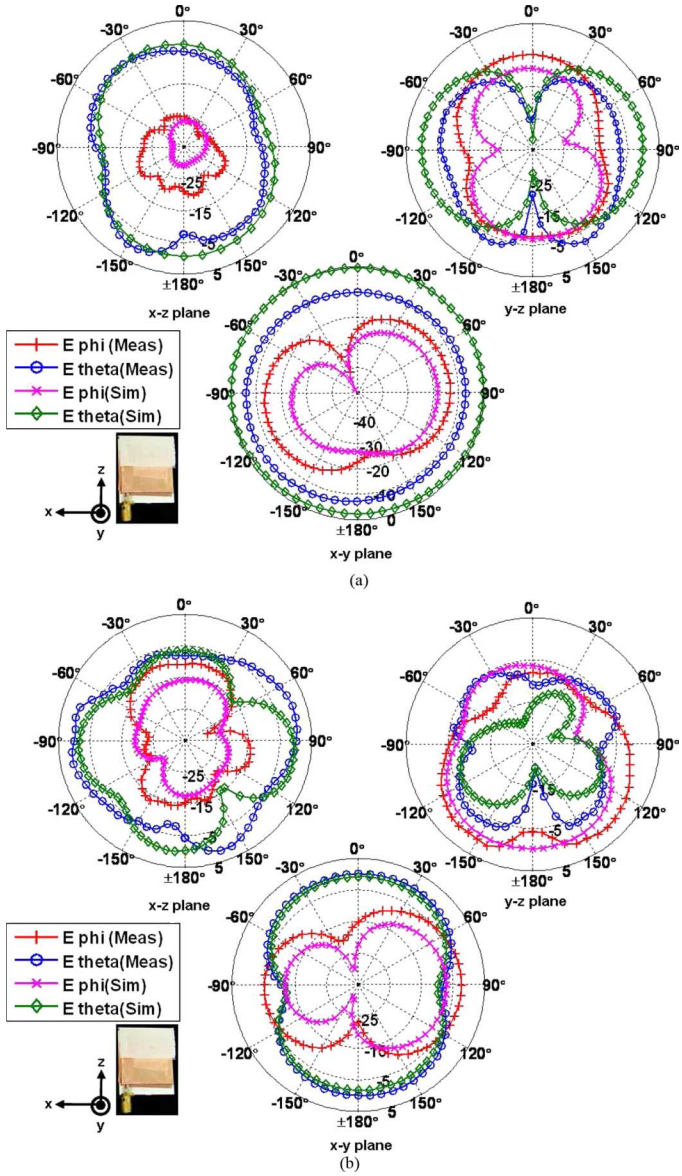

Fig. 22. Simulated and measured radiation patterns of the dual-band antenna: (a) 2.4 GHz and (b) 5.2 GHz.

between the simulation and the measurement results was observed. The simulated and the measured peak gains of the antenna for 2.4 GHz and 5.2 GHz were found as 1.47 dBi and 0.52 dBi, and 3.9 dBi and 2.92 dBi, respectively. The radiation pattern at 2.4 GHz is a dipole like pattern with a null along z axis since only the vertical current elements, labeled as s and h_2 in Fig. 17, contribute to the radiation while the fields of the horizontal components, labeled as l_2 and l_3, cancel each other. On the other hand, the pattern at 5.2 GHz has two nulls along approximately $\varphi = 45^\circ$ and $\varphi = 135^\circ$ axes due to the existence of orthogonal resonators for the 5 GHz band.

V. Conclusion

In this paper, a conformal antenna structure printed on a rigid-flex multilayer substrate is presented. The high-level integration of the antenna to the module package has been studied by considering the effects of an on-board shielding metal case. Furthermore, the transformation of the 5 GHz single-band antenna to a 2.4/5 GHz dual-band antenna has been introduced. The measured results obtained for the fabricated prototypes of both the single-band and dual-band antennas have been presented. It has been shown that conformal antennas on rigid-flex substrates can provide a novel solution to the antenna integration problem for mobile applications.

Acknowledgment

The authors would like to thank Per. O. Iversen and K. Rutkowski from Satimo, Kennesaw, GA, for providing the far-field measurements of the antennas.

References

[1] K. Brownlee, S. Bhattacharya, K. Shinotani, C. Wong, and R. Tummala, "Liquid crystalline polymers (LCP) for high performance SOP application," in *Proc. 8th Int. Symp. Adv. Packag. Mater.*, Mar. 2002, pp. 249–253.

[2] W. Yun, V. Sundaram, and M. Swaminathan, "High-Q embedded passives on large panel multilayer liquid crystalline polymer-based substrate," *IEEE Trans. Adv. Packag.*, vol. 39, no. 3, pp. 580–591, Aug. 2007.

[3] A. Bavisi, S. Dalmia, M. Swaminathan, G. White, and V. Sundaram, "Chip-package codesign of integrated voltage-controlled oscillator in LCP substrate," *IEEE Trans. Adv. Packag.*, vol. 29, no. 3, pp. 390–402, Aug. 2006.

[4] R. Bairavasubramanian and J. Papapolymerou, "Fully canonical pseudo-elliptic bandpass filters on multilayer liquid crystal polymer technology," *IEEE Microwave Wireless Compon. Lett.*, vol. 17, no. 3, pp. 190–192, Mar. 2007.

[5] W. Yun, V. Sundaram, and M. Swaminathan, "A triple balanced mixer in multilayer liquid crystalline polymer (LCP) substrate," in *Proc. IEEE 57th Electron. Compon. Technol. Conf.*, May 2007, pp. 2000–2005.

[6] M. M. Tentzeris *et al.*, "3-D-Integrated RF and millimeter wave functions and modules using liquid crystal polymer (LCP) system-on-package technology," *IEEE Trans. Adv. Packag.*, vol. 27, no. 2, pp. 332–340, May 2004.

[7] M. Swaminathan, A. Bavisi, W. Yun, V. Sundaram, V. Govind, and P. Monajemi, "Design and fabrication of integrated RF modules in liquid crystalline polymer (LCP) substrates," in *Proc. 31st Annu. Conf. IEEE Indust. Electron. Soc.*, Nov. 2005, pp. 2346–2351.

[8] Front-end modules on multilayer organic substrates [Online]. Available: http://www.jacketmicro.com/technology/applications.php

[9] S. Brebels *et al.*, "SOP integration and codesign of antennas," *IEEE Trans. Adv. Packag.*, vol. 27, no. 2, pp. 341–351, May 2004.

[10] R. Li *et al.*, "Design of compact stacked-patch antennas in LTCC multilayer packaging modules for wireless applications," *IEEE Trans. Adv. Packag.*, vol. 27, no. 4, pp. 581–589, Nov. 2004.

[11] Y. P. Zhang, "Integrated circuit ceramic ball grid array package antenna," *IEEE Trans. Antennas Propag.*, vol. 52, no. 10, pp. 2538–2544, Oct. 2004.

[12] N. Altunyurt, M. Swaminathan, V. Sundaram, and G. White, "Conformal antennas on liquid crystalline polymer substrates for consumer applications," in *Proc. IEEE Asia Pacific Microw. Conf.*, Dec. 2007, pp. 471–474.

[13] N. Altunyurt, R. Rieske, M. Swaminathan, and V. Sundaram, "Conformal WLAN/WiMAX antenna on rigid-flex liquid crystalline polymer based substrate," in *Proc. IEEE Radio Wireless Symp.*, Jan. 2009, pp. 19–22.

[14] J. Y. Chen, C. U. Huang, H. J. H. Chen, C. F. Jout, and S. R. S. Huang, "Folded dual-band (2.4/5.2 GHz) antenna fabricated on silicon suspended parylene membrane," in *Proc. IEEE Asia Pacific Microwave Conf.*, Dec. 2005, pp. 2346–2351.

[15] S. W. Bae, H. K. Yoon, W. Kang, Y. J. Yoon, and C. H. Lee, "A flexible monopole antenna with band-notch function for UWB systems," in *Proc. IEEE Asia Pacific Microwave Conf.*, Dec. 2007, pp. 1–4.

[16] L. Ma, R. M. Edwards, S. Bashir, and M. I. Khattak, "A wearable flexible multi-band antenna based on a square slotted printed monopole," in *Proc. 2008 Loughborough Antennas Propagat.Conf.*, Mar. 2008, pp. 345–348.

[17] S. W. Su, K. L. Wong, C. L. Tang, and S. H. Yeh, "Wideband monopole antenna integrated within the front-end module package," *IEEE Trans. Antennas Propag.*, vol. 54, no. 6, pp. 1888–1891, Jun. 2006.

[18] High frequency structure simulator (HFSS) [Online]. Available: http://www.ansoft.com

[19] G. E. White, M. Swaminathan, V. Sundaram, and S. Dalmia, "Integrated passive devices fabricated utilizing multilayer organic laminates," U.S. Patent 6 900 708.

[20] W. L. Weeks, "Propagation constants in rectangular waveguide partially filled with dielectric (Correspondence)," *IEEE Trans. Microwave Theory Tech.*, vol. 7, no. 2, p. 294, Apr. 1959.

[21] D. Pozar, *Microwave Engineering*. Hoboken, NJ: Wiley, 2005, pp. 278–300.

Nevin Altunyurt (S'07) received the B.S. degree in electrical and electronics engineering from Middle East Technical University, Ankara, Turkey, in 2005 and the M.S. degree in electrical and computer engineering from Georgia Institute of Technology, Atlanta, in 2007. Currently, she is pursuing the Ph.D. degree at the Epsilon Group at the Georgia Institute of Technology.

Her research interests include miniaturization and system-on-package integration of antennas for WLAN/WiMAX and millimeter wave applications. Her Ph.D. also focuses on the characterization of magneto-dielectric materials and their application to antenna miniaturization.

Ralf Rieske received the Diploma (corr. M.S.E.E.) in electrical engineering with focus on precision engineering and the Ph.D. degree in the field of electronic packaging from Technische Universität Dresden, in 2002 and 2006, respectively.

He made scientific contributions in the field of the electro-optical circuit board. His industrial experiences include automotive lighting with Hella as well as preparation and characterization of ultra-thin wafers with Infineon/Qimonda. During his postdoctoral studies he spent a research semester at the Packaging Research Center (PRC) of the Georgia Institute of Technology, Atlanta, where he has been involved in the research on embedded passive components for mixed signal system-on-package organic packaging. He is currently scientific staff at the Electronics Packaging Laboratory at TU Dresden, where he is leading Photonics Packaging Group. His recent research focuses on nano and microtechnologies for system integration.

Dr. Rieske is a member of the VDE (German Association for Electrical, Electronic & Information Technologies).

Madhavan Swaminathan (M'95–SM'98–F'06) received the B.E. degree in electronics and communication from the University of Madras, Chennai, India, and the M.S. and Ph.D. degrees in electrical engineering from Syracuse University, Syracuse, NY.

He is currently the Joseph M. Pettit Professor in Electronics in the School of Electrical and Computer Engineering, Georgia Tech, the Associate Director of the SRC Interconnect and Packaging Center and directs the design activities at the Packaging Research Center. He was the Deputy Director of the Packaging Research Center, Georgia Tech from 2004 to 2008. He is the co-founder of Jacket Micro Devices, a company specializing in integrated devices and modules for wireless applications and the founder of E-System Design, an EDA company focusing on CAD development for integrated microsystems. Prior to joining Georgia Tech, he was with the Advanced Packaging Laboratory at IBM working on packaging for super computers. He has over 300 publications in refereed journals and conferences, has co-authored three book chapters, has 17 issued patents, and has several patents pending. He is also the principal author of the book "Power Integrity Modeling and Design for Semiconductors and Systems, Prentice Hall, 2007" and co-editor of the book "Introduction to System on Package (SOP), McGraw Hill, 2008". While at IBM, he reached the second invention plateau. His research interests are in mixed signal micro-system and nano-system integration with emphasis on design, CAD, electrical test and new architectures.

Dr. Swaminathan has been a guest editor for the IEEE TRANSACTIONS ON ADVANCED PACKAGING and IEEE TRANSACTIONS ON MICROWAVE THEORY AND TECHNIQUES. He was the Associate Editor of the IEEE TRANSACTIONS ON COMPONENTS AND PACKAGING TECHNOLOGY. He is the recipient of the 2002 Outstanding Graduate Research Advisor Award from the School of Electrical and Computer Engineering, Georgia Tech and the 2003 Outstanding Faculty Leadership Award for the mentoring of graduate research assistants from Georgia Tech. He is also the recipient of the 2003 Presidential Special Recognition Award from IEEE CPMT Society for his leadership of TC-12 and the IBM Faculty Award in 2004 and 2005. He has also served as the co-author and advisor of a number of outstanding student paper awards at EPEP'00, EPEP'02, EPEP'03, EPEP'04, EPEP'08, ECTC'98, ECTC'08, APMC'05, and the 1997 IMAPS Education Award. He is the recipient of the Shri. Mukhopadyay best paper award at the International Conference on Electromagnetic Interference and Compatibility (INCEMIC), Chennai, India, 2003, the 2004 best paper award in the IEEE Transactions on Advanced Packaging, the 2004 commendable paper award in the IEEE Transactions on Advanced Packaging and the best poster paper award at ECTC'04 and '06. In 2007, Dr. Swaminathan was recognized for his research through the Technical Excellence Award given by Semiconductor Research Corporation (SRC) and Global Research Corporation (GRC). He served as the Co-Chair for the 1998 and 1999 IEEE Topical Meeting on Electrical Performance of Electronic Packaging (EPEP), served as the Technical and General Chair for the IMAPS Next Generation IC & Package Design Workshop, serves as the Chair of TC-12, the Technical Committee on Electrical Design, Modeling and Simulation within the IEEE CPMT society and was the Co-Chair for the 2001 IEEE Future Directions in IC and Package Design Workshop. He is the co-founder of the IMAPS Next Generation IC & Package Design Workshop and the IEEE Future Directions in IC and Package Design Workshop. He also serves on the technical Program committees of EPEP, Signal Propagation on Interconnects workshop, Solid State Devices and Materials Conference (SSDM), Electronic Components and Technology Conference (ECTC), and International Symposium on Quality Electronic Design (ISQED). He is the founder of Electrical Design of Advanced Packaging and Systems, a Signal Integrity Symposium in the Asian region.

Venky Sundaram received the B.S. degree in metallurgical engineering from Indian Institute of Technology, Bombay, India, and the M.S. degree in ceramic and materials engineering and the Ph.D. degree in materials science and engineering from the Georgia Institute of Technology, Atlanta.

He is the Director of Research at the Georgia Tech Packaging Research Center and a senior research faculty in the School of Electrical and Computer Engineering. He has leadership responsibility for SOP (system-on-a-package) Integration Research and Several Large Industry Consortia and Contract Programs requiring the establishment of center wide research programs development and collaborations with global industry and U.S./international universities and research groups. His research expertise includes SOP integration research and development, next generation substrate and assembly technologies, multi-mega function module technologies for electronic and bio-electronic systems. He has over 12 years experience in advanced packaging technologies including SOP, SiP, high-density microvia substrates, thin film wiring, and embedded actives/passives. He is also the co-founder of Jacket Micro Devices, a RF module technology startup and frequently consults for semiconductor and packaging companies worldwide. He has more than 75 publications, five U.S. and international patents, and multiple patents pending in SOP substrate technology and RF/Digital packaging.

Dr. Sundaram is a member of the High Density Substrate Technical Committee (TC-6) of IEEE-CPMT society.